IN-SITU STRESS ESTIMATION IN OFFSHORE EASTERN MEDITERRANEAN WITH FINITE ELEMENT ANALYSIS

Anna Kyriacou[1], Panos Papanastasiou[2] and Ernestos Sarris[3]

Department of Civil and Environmental Engineering

University of Cyprus

Nicosia 1678, Cyprus

[1]e-mail: kyriacou.anna@ucy.ac.cy; web page: http://www.ucy.ac.cy/cee/en/

[2] e-mail: panospap@ucy.ac.cy; web page: http://www.ucy.ac.cy/cee/en/

[3]e-mail: esarris@ucy.ac.cy; web page: http://www.ucy.ac.cy/cee/en/

Keywords: Insitu stresses, geomechanics, tectonic basin, Levantine basin, offshore drilling.

Abstract. *The objective of this study was to evaluate/estimate numerically the in-situ stress field in a tectonically active marine sedimentary basin. The Levantine basin in Eastern Mediterranean which is currently explored for gas and oil reservoirs is used as a case study. The study was based on elasticity and poroelasticity constitutive equations that were solved numerically by the finite element method. The model simulated a basin area initially at rest and then loaded by active tectonic movement of the plates over the geological time. The effect of boundary conditions and initial conditions were studied along with other important parameters that influence the problem such as the interface strength of fault surfaces and the plate movement. In the active tectonic regime the horizontal stress increases in such extent that it can be compared with the vertical stress. The adhesive behavior between the walls of a fault can cause interlocking resulting to even larger horizontal stress values. Smaller stresses are generated in sliding conditions between the fault surfaces due to the dissipated energy in the sliding process. Finally, the stress distributions become highly complex with stress rotation and arching closer to the fault.*

1 INTRODUCTION

In this paper we present the modeling of the in-situ stress state in the Levantine sedimentary basin which is characterized by tectonic movement and the presence of a deformation front in fault areas. Information such as insitu stresses and rock strength is needed for the design of wellbore stability during drilling, to predict sanding and to avoid damages in the casing and formation during production and reservoir depletion [1]. Drilling parameters, such as mud weight or the optimal orientation of the wellbore, require knowledge of the in-situ stresses and mechanical behavior of the rock[2]. The lack of these kind of data in exploratory areas with insufficient constraints for the geological model, increases the risk of wellbore failure and hence the cost. The ability of predicting the geomechanical behavior of the column rock that is going to be drilled is a desire scenario for the oil industry. Furthermore, knowledge of the ambient stress field is important in elucidating tectonic processes.

The present models use concepts from elasticity and poroelasticity theory in numerical models to compute the stationary stresses response of the formation that is submitted to effective compressive vertical stresses generated by the sea water weight and the gravity loading of the lithology of the sedimentary basin. Computational modeling is a step further necessary to understand the behavior of the stress field in a tectonically active area with complex boundary and loading conditions. The numerical solution is obtained using finite element analysis performed by Plaxis [3]. This study presents a novel approach for estimating all the components of the in-situ stresses in a tectonically active basin which are very different from those obtained based on the usual assumption of gravity loading of a basin at rest.

In the next section we present the model describing the geometry, the rock properties and the discretized domain. Section 3 presents the results for an elastic and poroelastic analysis in rest and active tectonic conditions and for different fault sliding conditions. The main findings and conclusions are summarized in section 4.

2. NUMERICAL MODEL

2.1 Basics of poroelasticity theory

The basic theory of poroelasticity was initially introduced by the pioneering work of Biot [4]. Since then many researchers have contributed to further developments. A comprehensive review of the theory of poroelasticity can be found in Detournay and Cheng [5]. The theory is commonly applied to soil mechanics problems especially for consolidation problems. The elastic response of the porous medium is given by the elastic strain rate and the elastic fluid mass content. These two parameters are related to the rates of total stress and pore pressure through isotropic constitutive equations that involve four material coefficients, namely: (a) the drained young's modulus E (b) the drained Poisson ratio ν, (c) the undrained Poisson ratio ν_u and (d) the Skempton coefficient, B. By definition the total stresses are related to the effective stresses through:

$$\sigma_{ij}^{'} = \sigma_{ij} - ap \tag{1}$$

where, σ_{ij}' is the effective stress, which is assumed to govern the deformation and failure of the rock. The poroelastic Biot constant α, is independent of the fluid properties and it is defined as:

$$\alpha = \frac{3(\nu_u - \nu)}{B(1-2\nu)(1+\nu_u)} = 1 - \frac{K}{K_s} \tag{2}$$

where, K is the bulk modulus of the matrix and Ks is the bulk modulus of the solid grains. An important distinction when applying the formulation to rock is that the compressibility of the constitutive materials must be considered. For soils B and α are equal to unity but in rocks are significantly less than one.

For the linear elastic case the constitutive relation may be expressed as a linear relation between small changes in strain and small changes in the effective stresses:

$$\delta\varepsilon = D_e \delta\sigma' \tag{3}$$

where, D_e is the elastic stiffness matrix.

2.1 Geometry of the Model

The geometry that was used to perform the large scale model simulations was constructed from the geophysical section shown in Figure 1. The sedimentary layers and the deformation front, which separates the Levantine basin from the Hecateaus rise (boundary of the African and Eurasian plates), can be delineated from seismic data [6,7]. Furthermore, it is shown that the basin on the left side of the deformation front has an approximate depth of 2 km below sea level while on the right side of the front it decreases to a depth of 1 km below sea level. Another important feature of Figure 1 is the distinction of the subsurface beddings of the sedimentary basin. As it is seen and expected, the beddings are nearly horizontal at a large scale. These horizontal beddings were created in different geological times, also shown in Figure 1.

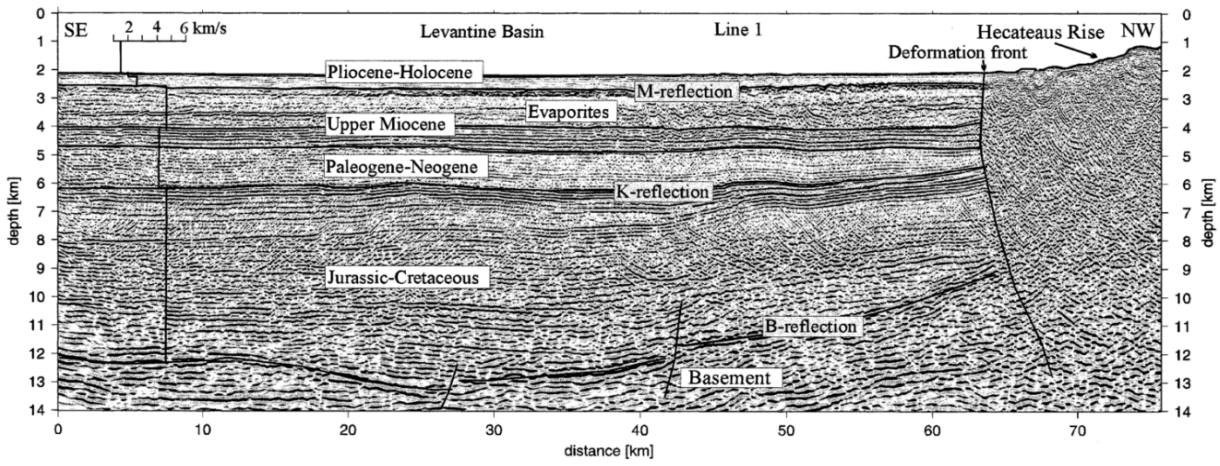

Figure1. Geological section interpreted from pre-stack depth-migrated seismic reflection image [6,7].

The geometrical model that was constructed by using the above geophysical information is shown in Figure 2. In order to avoid boundary effect problems, the length on the right side of the deformation front of the model was extended by 20 km assuming that the depth of the water will remain constant to 1 km. The reference origin of the

model is located at the left upper end of the geometry.

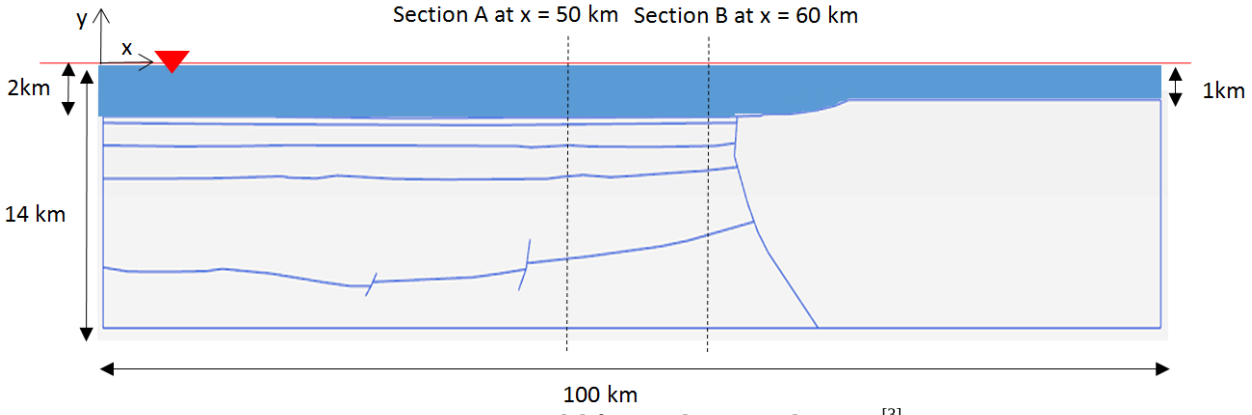

Figure 2: Geometry model for simulation in Plaxis2D [3].

In Figure 2 we have inserted two lines/sections located at 50 km and 60 km from the left side of the models. These two lines are the sections where we will analyze the stress field in line plots. The selection of these locations represents results for the areas far and close to the deformation front.

2.2 Stratigraphy and Material Characterization

One of the many difficulties for the construction of the real scale model, was the complete lack of drilling data and material properties for each sedimentary layer. The material rock properties needed for this investigation are the rock densities or the specific weights (γ_{unsat}, γ_{sat}), the Young modulus (E), the Poisson ratio (v), the porosity n (%), the interface strength coefficient (Rinter) and the earth lateral coefficient (Ko,x). Furthermore, the simulations were performed for the elastic and poroelastic constitutive behavior. For the large scale data we ignore any plastic or poroplastic deformation that would need additional material data such as cohesion c, friction angle, φ and dilation angle ψ.

In order to extract the aforementioned material properties for each sedimentary layer we have constructed the stratigraphy from two resources. The stratigraphy of the above model (Figure 1) was partly constructed by using data from the geophysical results [6,7]. Figure 3 shows the created stratigraphy of the Levantine basin. On the left side of the stratigraphy the age and thickness of the sedimentary layers is shown. The types of materials encountered in the subsurface as a function of depth is shown on the right side.

The first sedimentary layer from sea bed to 1 km depth is from Pliocene to Recent age (5.3-0.01 Ma?) and consists of fine distal facies clastic sediments from the Nile Delta. The second layer has Messinian evaporites (1.4 km thickness) and is dominated by rock salt [6,7]. The third layer is from Paleogene to Neogene age. These layers are characterized as mudstones and sandstones with 2 km thickness. The fourth layer consists of mudstones, marlstones and small amounts of shale with 6 km thickness. Finally, the last layer is considered to be the basement and the types of material found in this rock are of oceanic origin.

After the identification of the sedimentary layers (geometry/material characterization) of the Levantine basin we define the material properties for the simulations. Unfortunately, actual in-situ material properties of the area are not yet officially published and the only values found are for specific gravities and porosities, borrowed from the literature and laboratory testing results in regions that can be correlated with the area under consideration.

Following the specification of the specific weight of each rock, the definition of the stiffness values for the Young modulus and Poisson ratio were obtained. With the known values of p-wave velocities for each bedding an approximate value of the Poisson ratio and Young modulus were estimated. In an elastic, isotropic, homogeneous solid the shear moduli G and compression index K can be determined from the velocity of compressional waves, V_p and shear waves V_s using the following relations [8].

$$V_p = \sqrt{\frac{K + 4G/3}{\rho}} \tag{4}$$

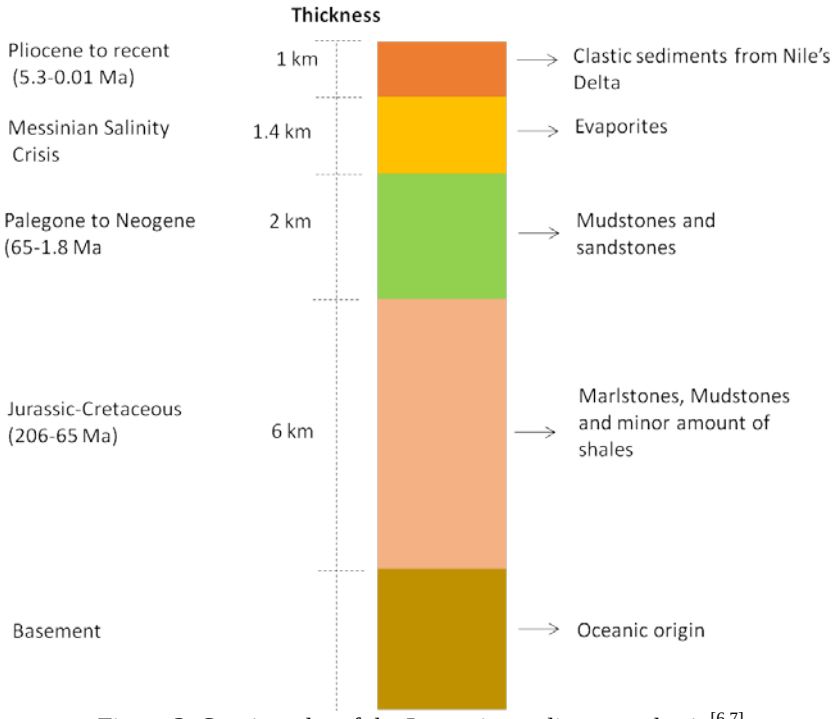

Figure 3: Stratigraphy of the Levantine sedimentary basin[6,7].

$$V_s = \sqrt{\frac{G}{\rho}} \tag{5}$$

It is obvious from these relations that Vp is always greater than Vs (when ν = 0.25, Vp/Vs =√3= 1.73) and that Vs=0 in a fluid. It is also often useful to consider relative rock stiffness directly as determined from seismic wave velocities. For this reason the so-called M modulus is

$$M = V_p^2 \rho = \mathrm{K} + \frac{4G}{3} \tag{6}$$

Beddings	γd (kN/m^3)	γsat (kN/m^3)	n (%)	e	ν	Vp (10^{3}m/s)	Vs (10^{3}m/s)	E (GPa)
1	22	24	31	0.45	0.25	2500	1443.38	11.68
2	20	22	4	0.04	0.32	4300	2212.33	26.34
3	21	23	18	0.22	0.2	3900	2388.25	29.31
4	23	25	16	0.19	0.25	4500	2598.08	39.56
5	25	27	16	0.19	0.4	4500	1837.12	24.08

Table 1. Material properties of the sedimentary layers

The Poisson's ratio can also be determined from Vp and Vs utilizing the following relation

$$\nu = \frac{V_p^2 - 2V_s^2}{2\left(V_p^2 - V_s^2\right)} \tag{7}$$

2.3 Discretization

The finite elements used for the discretization of the basin are 15-node soil element and for the fault deformation are 10-node interface elements. The dimensions of this model are large and therefore a very large number of elements is needed in areas with sharp deformation in order to derive accurate results. The accuracy and area of interest does not focus only on the interface but in the entire sedimentary domain. The final mesh was a result of a repetitive local refinement in places where high stress and deformation were expected to develop. These refinements are near the interface, the boundaries and the lines that define the change of the rock type. Figure 4 shows the finite element discretization details in the whole domain for the model created for the numerical analysis.

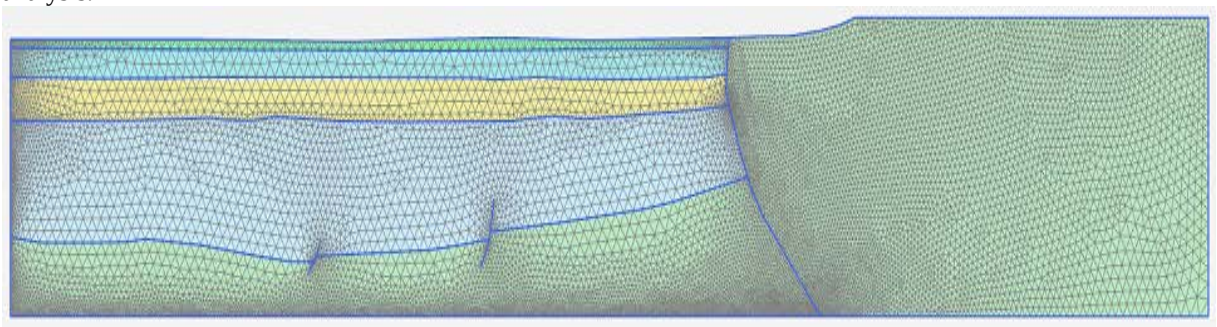

Figure 4: Final finite element mesh of the large scale models.

3 RESULTS

3.1 Poroelasticity vs Elasticity at Rest

The simulation with the two different theories, elasticity and poroelasticity, were performed to investigate any differences and similarities between the classical method used by the industry to convert the sea water weight as equivalent load and the non trivial that applies the sea water and solves the coupled deformation-flow problem with finite elements. In the following analysis the stresses obtained with the poroelastic model are compared with the stresses created from the elastic model.

Figure 5 shows the comparison for the vertical stress profile between the elastic and poroelastic models at rest. With the term "at rest" we mean that only the gravity load and the sea water load are applied. In this figure we also included the effective vertical stress distribution for comparison reasons. No inclusion of plate tectonic movement is discussed in this comparison. We observe that the two stress distributions begin at the same magnitude of vertical stress verifying that the boundary conditions of the two models have been applied correctly. As the depth increases the magnitude of the poroelastic vertical stress also increases delineating the effect of pore pressure and saturated rock density on the vertical stress component σ_{yy}. A further comparison, shows that the effective vertical stress of the poroelastic model is 45% lower than the stress profile of the elastic model.

Figure 6 presents the horizontal stress distribution at rest for the elastic and poroelastic analysis. In this analysis we also included the effective horizontal stress distribution. We observe that the stress field created for the horizontal stress component is highly affected by the presence of pore pressure in the modeling, compared to the influence observed in the vertical stress component. In the elastic case the application of the loading in a 2nd step created a discontinuity at the interfaces of the layers with different stiffness. In the case of the poroelastic case the initial condition and loading were applied in one step which results in the reference of the undeformed configuration. A comparison, between the effective horizontal stress distribution of the poroelastic with the elastic model shows again that the stress magnitude is smaller about 45%. By comparing the effective out of plane horizontal stress distribution of the poroelastic with the elastic model, it appears that the stress magnitude is smaller about 40%.

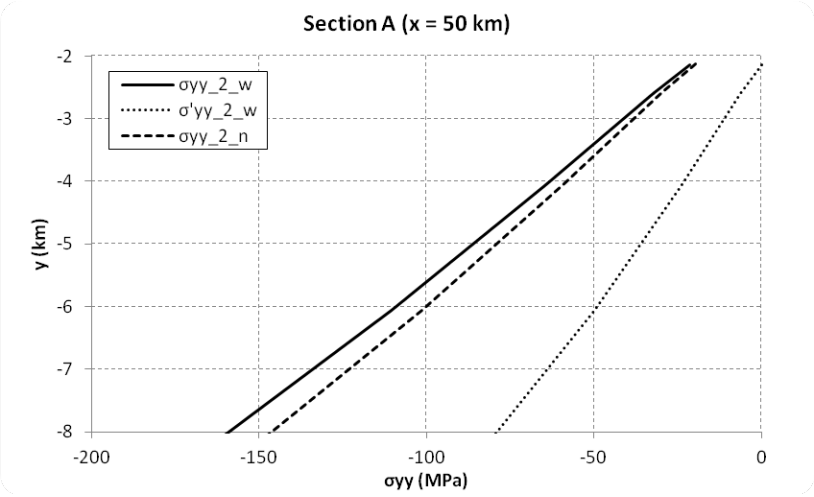

Figure 5: Comparison of the vertical stress distribution between an elastic (dashed line) and poroelastic analysis for total stress (solid line) and effective stress (dotted line) at rest.

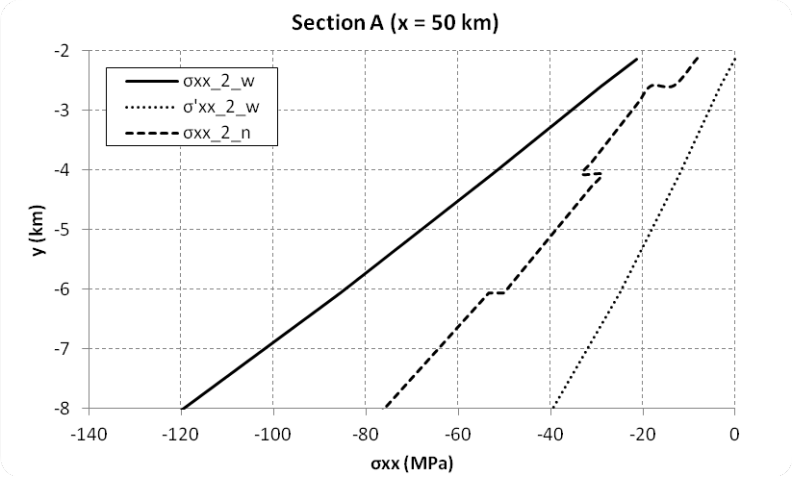

Figure 6: Comparison of the horizontal stress distribution between an elastic (dashed line) and poroelastic analysis for total stress (solid line) and effective stress (dotted line) at rest.

The above calculations were based on Terzachi's effective principle which is equivalent to poroelastic analysis with Biot coefficient a=1.0. If a more realistic Biot coefficient for strong rock is assumed a=0.5 then the differences between total elastic and poroelastic horizontal stresses (Fig.5, 6) would be much smaller.

A closer examination of the differences obtained between the elastic and poroelastic analysis reveals that the vertical total stress component is not influenced significantly by changing the analysis from elastic to poroelastic. The differences observed are 9.37% higher for the poroelastic case in the deeper layers. The horizontal total stress component of the poroelastic model is higher by 37.5% and the out of plane stress component is 41.69% higher in the poroelastic analysis. This result is of course directly related with the set of material data used for the simulations. However, if the above analysis was repeated with different set of data the physical interpretation would remain unaltered. The poroelastic modeling in the determination of the in-situ stress regime, which is usually ignored by classical simulators, produces a more realistic stress regime that is needed for the analysis of wellbore stability. According to this study if a stability analysis of the wellbore was going to be performed in drained conditions with the stress components obtained with the theory of elasticity it would produce significant overestimation of the tangential stress which is responsible for the wellbore breakouts. Drained conditions analysis with effective stresses may lead to less conservative calculations showing more stable wellbore than in the case of the elastic model. For this reason the influence of the pore pressure and the direct application of the appropriate loads (i.e. gravity load and sea water weight) must be considered in the analysis of the stress regime estimation and not be ignored by simplified analysis.

3.2 Poroelasticity vs Elasticity in an Active Tectonic Regime

The next set of comparisons between the two different theories, elasticity and poroelasticity deals with the case of a highly active tectonic regime. In the following analysis the stresses obtained with the poroelastic model are compared with the stresses created from the elastic model after the application of 750 m displacement that represents the total movement after 50000 years over the geologic time based on the estimated movement every year.

Figures 7 to 8 show the comparison for (a) the vertical stress profile and (b) the horizontal stress distribution. Each of these figures contains the elastic total stress, the poroelastic total stress and the poroelastic effective stress.

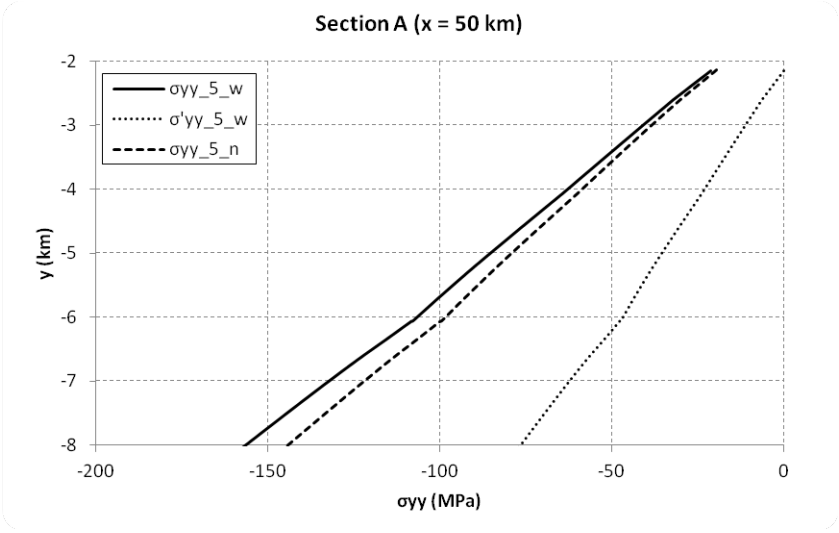

Figure 7: Vertical stress distribution for elastic (dashed line) and poroelastic analysis for total stress (solid line) and effective stress (dotted line) in an active tectonic regime after 750 m horizontal displacement.

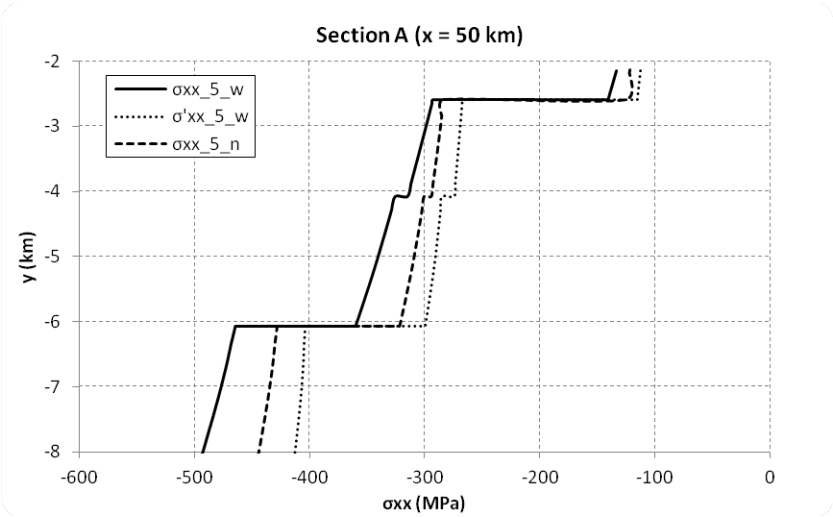

Figure 8: Horizontal stress profile for elastic (dashed line) and poroelastic analysis for total stress (solid line) and effective stress (dotted line) in an active tectonic regime after 750 m horizontal displacement.

A comparison between the cases where the stresses are obtained in active and inactive tectonic regimes shows that the vertical stress distribution appears to be insensitive to the plate movement. However, the horizontal stress profiles (plane and normal to plane) are highly influenced with the plate movement. We found that the stress magnitudes after the application of the boundary condition that simulates the plate movement had increased dramatically. Nevertheless, the magnitude of the horizontal stress could be reduced to more realistic values of the order of the vertical stress if smaller horizontal displacement was applied, of the order of 250m.

3.3 The Influence of Interface Strength in an Active Tectonic Regime

The last set of comparisons is concerned with the influence of the interface sliding conditions at the fault. The parameter that expresses the interface strength in Plaxis is Rinter which is the ratio of the sliding resistance over the strength of the bulk rock. A small value of Rinter = 0.05 represents an almost free sliding behavior whereas the value Rinter = 1 represents the fully bonded condition. The presented results are from the area analysis close to the deformation front. The stress magnitudes used in these comparisons are obtained after the application of 750 m displacement boundary condition to simulate the plate movement.

Figures 9 and 10 show the comparison for (a) the vertical stress profile and (b) the horizontal stress profile for the case of interface strength that permits free sliding (Rinter = 0.05). Figure 11 shows the horizontal effective stress in the whole domain. Each of these figures contains the elastic total stress, the poroelastic total stress and the poroelastic effective stress profiles.

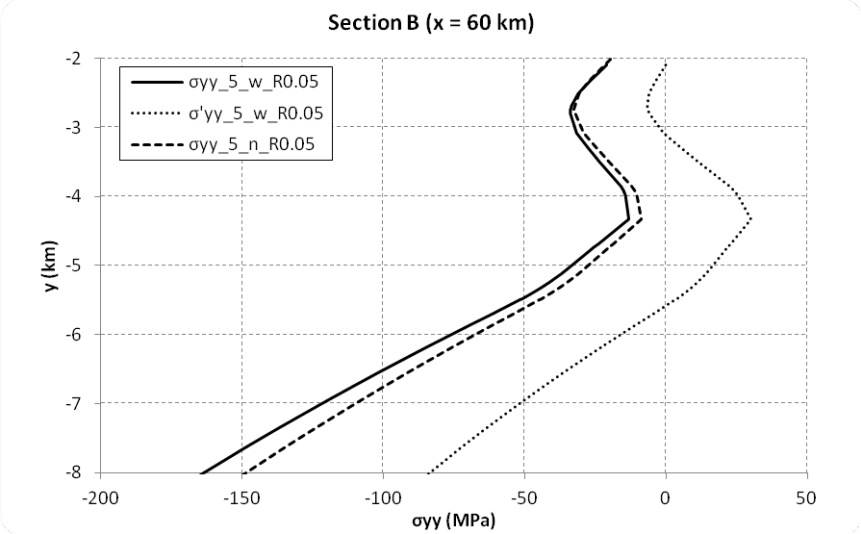

Figure 9: Vertical stress profile for elastic (dashed line) and poroelastic analysis for total (solid line) and effective stress (dotted line) in active tectonic regime after 750 m horizontal displacement for Rinter = 0.05.

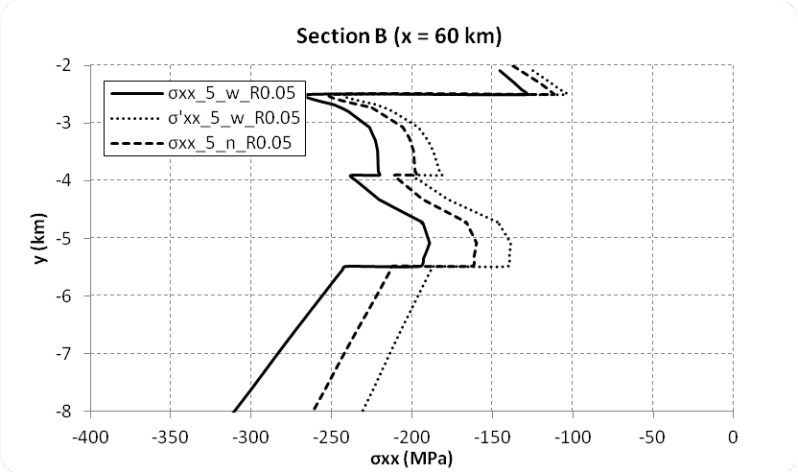

Figure 10: Horizontal stress profile for elastic (dashed line) and poroelastic analysis for total (solid line) and effective stress (dotted line) in active tectonic regime after 750 m horizontal displacement for Rinter = 0.05.

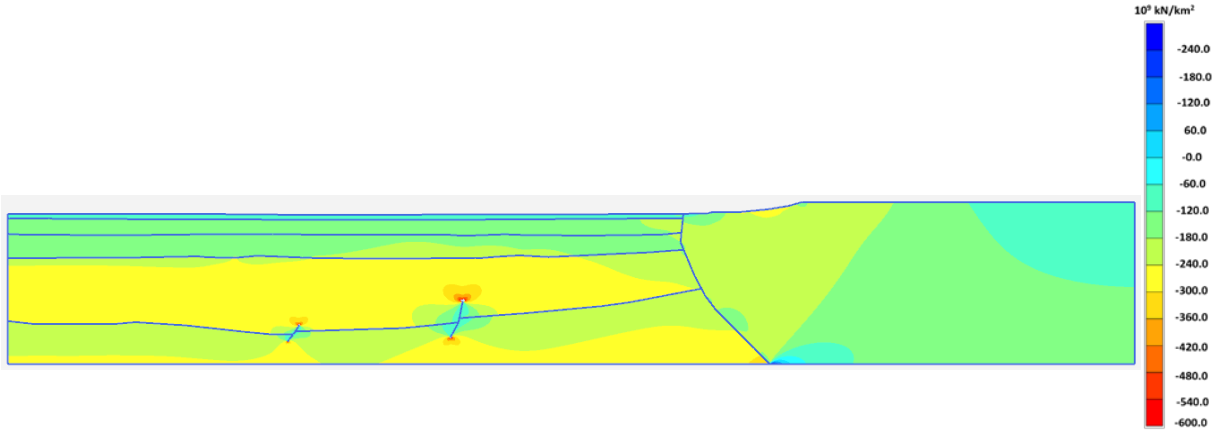

Figure 11: Horizontal effective stress field, σ'_{xx} for the poroelastic model in an active tectonic regime after 750 m displacement for Rinter =0.05.

Figures 12 and 13 show the comparison for (a) the vertical stress profile and (b) the horizontal stress profile for the case of interface strength that restricts sliding which simulates adhesive or fully bonded conditions (Rinter = 1).

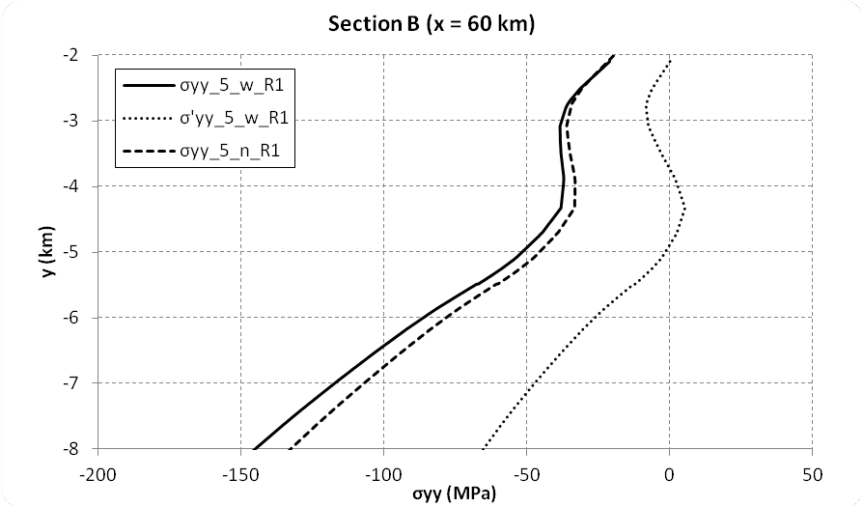

Figure 12: Vertical stress profile for elastic (dashed line) and poroelastic analysis for total (solid line) and effective stress (dotted line) in an active tectonic regime after 750 m horizontal displacement for Rinter = 1.

Figure 9 and 12 show arching condition at the depth of 4 Km resulting in vertical stress relief. It seems that the area near the fault (Fig.9) is characterized by stress rotation, arching and stress relief phenomena. The general conclusion that is drawn from Figures 9 and 10 which corresponds to free sliding and Figures 12 and 12 that represents the bonded behavior is that the horizontal stress distributions show smaller magnitudes and the vertical stress shows higher magnitudes for the case of free sliding (Rinter = 0.05). This finding is interpreted with the energy and work that is expended from the sliding process. The physically admissible behavior of free sliding dissipates energy that is created from the plate movement and as a result the horizontal stress magnitude is smaller than the case that the deformation front presents adhesive behavior.

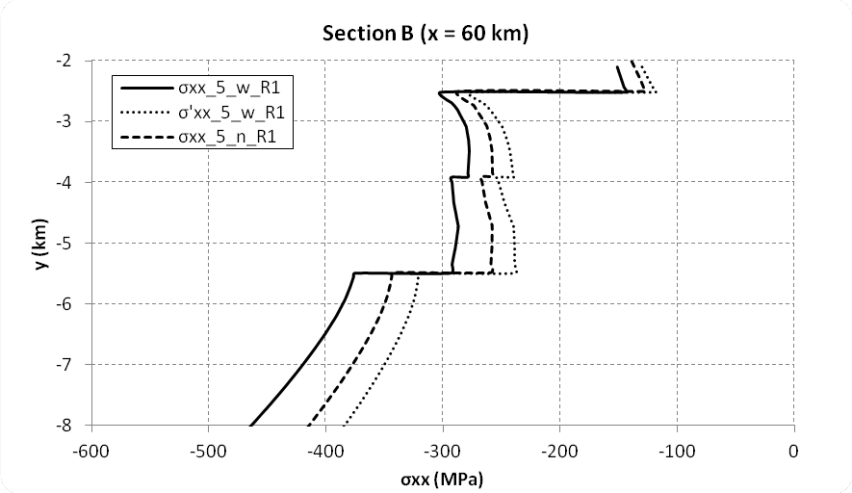

Figure 13: Horizontal stress profile for an elastic (dashed line) and poroelastic analysis for total (solid line) and effective stress (dotted line) in an active tectonic regime after 750 m horizontal displacement for Rinter = 1.

4. CONCLUSSION

The finite element analysis is a powerful tool for estimating the insitu stresses in abnormal stress environment such as in active tectonic areas. The information on insitu stresses are needed in many applications in petroleum engineering. We applied this knowledge to estimate the insitu stress in an exploration area in Eastern Mediterranean. The following conclusions are applied in other similar areas with tectonic movements.

1. Poroelastic analysis produces more realistic results especially for the case of the horizontal effective stress.
2. Tectonic movement increases the horizontal stress to a level comparable to the vertical insitu stress.
3. The insitu stresses developed near a fault are strong functions of the sliding conditions at the fault surface. Free sliding conditions result in smaller developed horizontal stress and higher vertical stress whereas fully bonded conditions results in higher horizontal stress.
4. The stress field near a fault is characterized by stress rotation, arching and stress relief phenomena that can be modeled only numerically at field scale conditions.

REFERENCES

[1] Papanastasiou P. (ed) (2004). "Petroleum Geomechanics", special issue *ASCE Int. J. Geomechanics*, 4 (1), ISSN 1532-3641.

[2] Papanastasiou P and Zervos A (2004). "Wellbore Stability: from linear elasticity to post-bifurcation modeling", *ASCE Int. J. Geomech*, 4(1), pp.2-12, (2004).

[3] Plaxis 2D (2010), Reference Manual.

[4] Biot, M.A. (1941). "General theory of three dimensional consolidation." *J. Ap. Phys.*, 12, 155-164.

[5] Detournay, E., and Cheng, A.H-D. (1993). "Fundamentals of poroelasticity." *Comprehensive Rock Engineering: Principles, Practice and Projects*, J.A. Hudson, ed., Pergamon Press, Oxford, UK , 2, 113-171.

[6] Vidal N., D. Klaeschen, A. Kopf, C. Docherty, and R. Von Huene, (2000a). "Krasheninnikov V.A., Seismic images at the convergence zone from south of Cyprus to the Syrian coast, Eastern Mediterranean". *Tectonophysics*, Vol. 329, pp. 157-170.

[7] Vidal N., J. Alvarez-Marrón, and D. Klaeschen, (2000b). "Internal configuration of the Levantine Basin from seismic reflection data (Eastern Mediterranean)". *Earth and Planetary Science Letters*, Vol. 180, pp. 77-89.

[8] Zoback, M.D., 2007. Reservoir Geomechanics. *Cambridge University Press*, New York.